International Journal of the Physical Sciences Vol. 6(28), pp. 6361-6372, 9 November, 2011
Available online at http://www.academicjournals.org/IJPS
DOI: 10.5897/IJPS10.223
ISSN 1992 - 1950 ©2011 Academic Journals

Review

Finite element analysis of a vertical reinforced earth wall

Faisal Ali* and Lee Chee Hai

Department of Civil Engineering, National Defense University of Malaysia, 50603 Kuala Lumpur, Malaysia.

Accepted 30 September, 2011

Reinforced earth wall system has become very popular because of its aesthetic value and ease of construction. In order to optimize the design, it is important to understand its behavior during and after construction. This can be achieved either through field instrumentation or numerical simulation. In this paper, a numerical simulation of a reinforced earth wall construction is described and a parametric study using a finite element method is conducted to investigate the performance of the wall during and after construction. Different types of boundary conditions are imposed and the behavior of the wall is evaluated based on certain stress and deformation criteria. The results show that if the wall is allowed to move laterally, horizontal pressures at the connection increases with the depth of overburden until a depth of 0.6 H (height of wall) is reached. Beyond 0.6 H, the horizontal pressure starts to reduce with further depth. If no lateral movement is allowed, the horizontal pressure line follow more or less the KO line until a depth of 0.6 H is reached. Below 0.6 H, the horizontal pressure starts to drop rapidly. The increasing compressibility of the foundation soil induces redistribution of stresses that results in larger tensile forces in the reinforcements at lower levels and smaller tensile forces at around 0.6 H depth of overburden. As the foundation becomes more compressible, the horizontal displacement of wall facing increases.

Key words: Anchor blocks, computer simulation, instrumentation, reinforced earth.

INTRODUCTION

In 1981, the Transport and Road Research Laboratory in United Kingdom patented the Anchored Reinforced Earth wall, which is another type of reinforced soil system. The major difference between the Reinforced Earth and the Anchored Reinforced Earth is that the Anchored Reinforced Earth has anchors attached at the free ends of the reinforcing elements whereas the Reinforced Earth has none. Jones and Pugh (2001) report the first application of the Anchored Reinforced Earth wall. Meanwhile, the application of reinforced soil system similar to Anchored Reinforced Earth is reported in other parts of the world. For example, the loop-shaped anchor system in Austria, the multi-anchor wall system in Japan and in Malaysia (Lee, 2004) (Figure 1). One of the advantages of this system is that it can be applied in soils which have relatively high fine-content such as residual soil (Bujang et al., 2008; Ali and Osman, 2008; Ali, 1993; Ali et al., 1992; Anderson et al., 1987; Normaniza et al., 2008).

The presence of anchor blocks would help to mobilize additional lateral resistance through bearing. Parallel to the rapid development and application of reinforced soil technique is the availability of the high speed computers with great computing power. This easy availability of powerful computers has spurred the growth in the application and sophistication of the numerical modeling technique. This application of this powerful numerical tool in the study of reinforced soil structures in turn leads to a greater in depth understanding of the behavior of reinforced soil structures.

*Corresponding author. E-mail: faisal.fas@gmail.com.

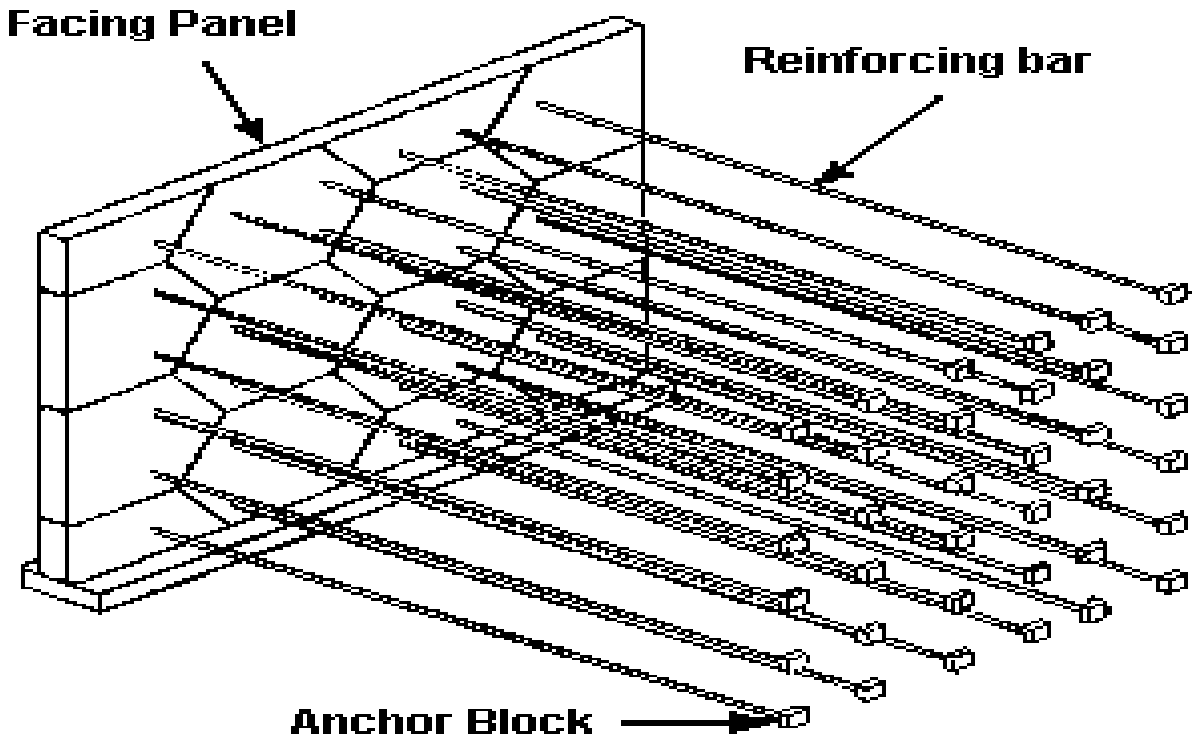

Figure 1. Schematic representation of an anchored reinforced earth wall.

Hence, the cost effectiveness of reinforced soil structures coupled with the advent of new materials and high speed computers have resulted in the phenomenal growth in the design, analysis and application of reinforced soil technology throughout the world. Despite the successive refinements in the design methodology or approach in reinforced earth, the fundamental design philosophy remains the same that is, it is based on the limit equilibrium method. The basic design assumptions of all these codes and manuals are that the reinforced soil structure is sitting on a firm ground or piled foundation and that there is little yielding of the lateral boundary. In other words, the present design methodology is unable to take into account the effects of yielding at the base and as well as facing the wall. Hence, if the wall is sitting on a compressible founding soil layer, the present design method is unable to capture the changes in the stresses in the reinforcing elements of the wall as a result of the yielding base. Likewise, if the facing of the wall is allowed to move laterally, the present design method is again unable to capture the changes in the tensile stresses developed in the reinforcing elements due to the lateral yielding. Therefore the main objective of this study was to investigate and determine the influence of the boundary conditions on the behavior of the anchored reinforced wall system. The boundary conditions investigated were the slope surcharge at the crest, the deformation at the facing and the deformation at the base of the wall.

FINITE ELEMENT MODEL

The finite element code used was called PLAXIS developed initially in the Technical University of Delft, Netherlands. The geometry of the finite element model based on the constructed and instrumented multi- anchor wall system is shown in Figure 2. The wall was divided into two tiers. The lower tier was 6.75 m high while the upper tier is 9.0m high and the total height of the wall was 15.75 m. The upper tier was off set from the lower by 1.5 m. Following the design, the length of the reinforcing bars was 9.9 m long for the bottom two layers while the rest of the bars were 10.9 m long. The vertical spacing of the reinforcing bars was constant at 0.75 m. The boundaries were sufficiently far away so that they have no significant influence on the behavior of the wall.

Mesh generation

The plot of the finite element mesh is shown in Figure 2. The mesh was generated by PLAXIS, which had the

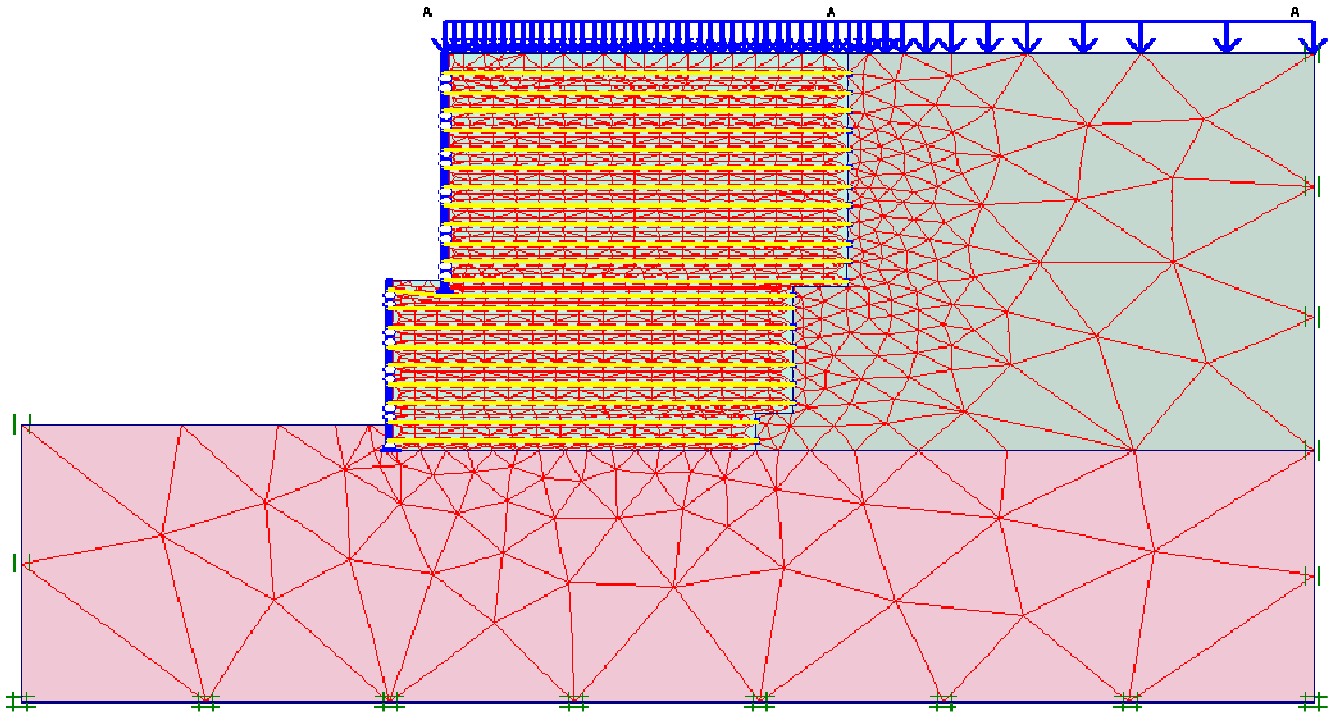

Figure 2. The geometry of the finite element model.

automatic mesh generation capability. The generation of the mesh was based on a robust triangulation procedure, which resulted in 'unstructured' meshes. These meshes might look disorderly, but the numerical performance of such meshes was usually better than regular (structured) meshes. To ensure reasonably accurate results, the global coarseness was set to medium level. However, for greater accuracy, the meshes between the layers of reinforcing bars were further refined locally. The finite element mesh generated for the analysis of the section consisted of 1319 elements, 4210 nodes and 3957 stress points.

Boundary conditions

The wall was resting on a firm foundation. The depth of the foundation was truncated at 10 m depth below which the boundary was fixed in both horizontal and vertical direction. The right boundary was fixed in horizontal direction but was allowed to move in the vertical direction. Likewise the left boundary was fixed in horizontal direction but was allowed to move in vertical direction. However, the boundary at the wall facing was allowed to move in both horizontal and vertical direction. The boundary conditions described above are shown in the finite element mesh in Figure 2.

Initial conditions

After the generation of the finite element mesh, the initial stress state needed to be specified. The initial conditions consisted of two modes namely the generation of initial water pressures and the generation of initial effective stress field. However, for this particular Nehemiah wall, the ground water was well below the base of the founding level and the backfill material was free draining. The water pressure was negligible. The initial stress field was generated for the ground below the founding level because the embankment was constructed subsequently.

Materials properties and models

In contrast to the composite model used in the late 70's, the discrete model was used for the present study. In the discrete model, each of the system components was distinctly and separately modeled. The components of the complete model consisted of foundation soil, pad footing, facing panels, backfill material, retained fill, reinforcing bars and the anchor blocks. In addition, soil structure interaction, the effects compaction and stage construction needed to be considered as well. The properties of each of the components and the modeling techniques involved were discussed subsequently.

Table 1. Material properties of the foundation soil.

Parameter	
Material model	Mohr-Coulomb
Type of material behavior	Drained
Dry soil weight γ_{dry} (kN/m^3)	18
Wet soil weight γ_{wet} (kN/m^3)	20
Permeability in hor. direction k_x (m/day)	1
Permeability in vert. direction k_y (m/day)	1
Young's modulus (constant) E_{ref} (kN/m^2)	80000
Poisson's ratio, ν	0.3
Cohesion (constant) c_{ref} (kN/m^2)	100
Friction angle, $\varphi°$	34
Dilatancy angle, $\psi°$	0
Interface strength reduction factor	1
Interface permeability	Neutral

Foundation soil

The Mohr-Coulomb soil model was chosen to model the foundation soil. This was an elastic perfectly-plastic soil model. The basic parameters of Mohr-Coulomb model were Young's modulus E', Poisson's ratio ν', cohesion intercept c', friction angleϕ' and dilatancy angle ψ. From the soil report, it was seen that the foundation soil was firm. The parameters adopted for the foundation soil is shown in Table 1. The Hardening soil model is an elastoplastic type of hyperbolic model, formulated in the framework of friction hardening plasticity. It was chosen over the Mohr-Coulomb model for several reasons. First, the Mohr-Coulomb model represents a first order approximation of soil behavior. It is useful for first analysis of problem considered as the computations tends to be very fast. However, the Mohr-Coulomb model allows only a constant value of young's modulus whereas for real soils, the stiffness is stress dependent. A basic feature of hardening soil model is the stress dependency of soil stiffness. Moreover, the hardening soil model represents a much more advanced model than the Mohr-Coulomb model.

Soil stiffness is described much more accurately by using three different input stiffnesses: the triaxial loading stiffness, E_{50} and the triaxial unloading stiffness. The parameters used for the hardening soil model were shown in the Table 2. The retained fill was normally constructed progressively lift by lift in consonance with the construction of the backfill. The retained fill was made up of material excavated from the original ground, which consisted mainly of residual soil of shale and sandstone origin. It is compacted to 90% proctor density in lifts of 375 mm thickness. In order to save computing time, the Mohr-Coulomb model was used to model the retained fill. The parameters used for the retained fill is shown in Table 3. The geoinclusion inserted at the back face of facing panel was made of expanded polystyrene. It had low density 0.15 kN/m^3 (0.2 kN/m^3 was adopted) and low E modulus of 300 kN/m^2. It was assumed to behave like the Mohr-Coulomb soil model.

Modeling of concrete components

The concrete components of the system consisted of the facing panels, leveling pad footing and the anchor blocks. They were modeled by beam element which had three nodes when used in conjunction with six-node soil element. The beam element had three degrees of freedom per node: two translational degrees of freedom (u_x and u_y) and one rotational degree of freedom (rotation in the x-y plane: ϕ_z).They were based on Mindlin's beam theory. This theory allowed beam deflections due to shearing as well as bending. In addition, the element could change length when an axial force was applied.

Facing panels

The facing panels were normally made of grade 30 precast concrete with nominal reinforcement. Each panel was loosely connected to another by a dowel bar in one panel inserted into the PVC tube embedded in another panel. The joints between the panels were therefore hinged rather than rigid. This hinged connection could be

Table 2. Material properties of granular backfill.

Parameter	
Material model	Hardening soil
Type of material behavior	Drained
Dry soil weight γ_{dry} (kN/m^3)	18
Wet soil weight γ_{wet} (kN/m^3)	20
Permeability in hor. Direction, k_x (m/day)	1
Permeability in vert. direction, $k_{y\ (}$m/day)	1
Secant stiffness in standard drained triaxial test E_{50ref} (kN/m^2)	16000
Tangent stiffness for primary oedometer loading, E_{oedref} (kN/m^2)	16000
Unloading/reloading stiffness Eur_{ref} (kN/m^2)	48000
Cohesion, c (kN/m^2)	100
Friction angle φ°	36
Dilatancy angle ψ°	0
Poisson's ratio for unloading/reloading ν_{ur}	0.2
Reference stress for stiffness p_{ref} (kN/m^2)	100
Power for stress-level dependency of stiffness (m)	0.5
Ko value for normal consolidation Konc	0.412
Failure ratio q_f/a_a	0.9
Interface strength reduction factor	0.67
Interface permeability	Neutral

Table 3. Material properties of retained fill.

Parameter	
Material model	Mohr-Coulomb
Type of material behavior	Drained
Dry soil weight γ_{dry} (kN/m^3)	18
Wet soil weight γ_{wet} (kN/m^3)	20
Permeability in hor. Direction, k_x (m/day)	1
Permeability in vert. direction, k_y (m/day)	1
Young's modulus (constant), E_{ref} (kN/m^2)	40000
Poisson's ratio, ν	0.3
Cohesion (constant) c_{ref} (kN/m^2)	1
Friction angle, φ°	30
Dilatancy angle, ψ°	0
Strength reduction factor inter.	1
Interface permeability	Neutral

modeled by the *beam hinge* option available in PLAXIS.

Anchor blocks

The anchor blocks were made of grade 30 concrete. Their sizes were standard block 200x200x100, enlarged blocks 400×200×100 and 600×200×100. As the finite element analysis was based on the plain strain concept, the wall was analyzed based on per linear meter run of wall. However, the blocks were individual isolated blocks separated from each other. An equivalent block of 1 m was determined based on the size and number of blocks per m run of wall. The equivalence was computed based on passive resistance surface area and the flexural stiffness.

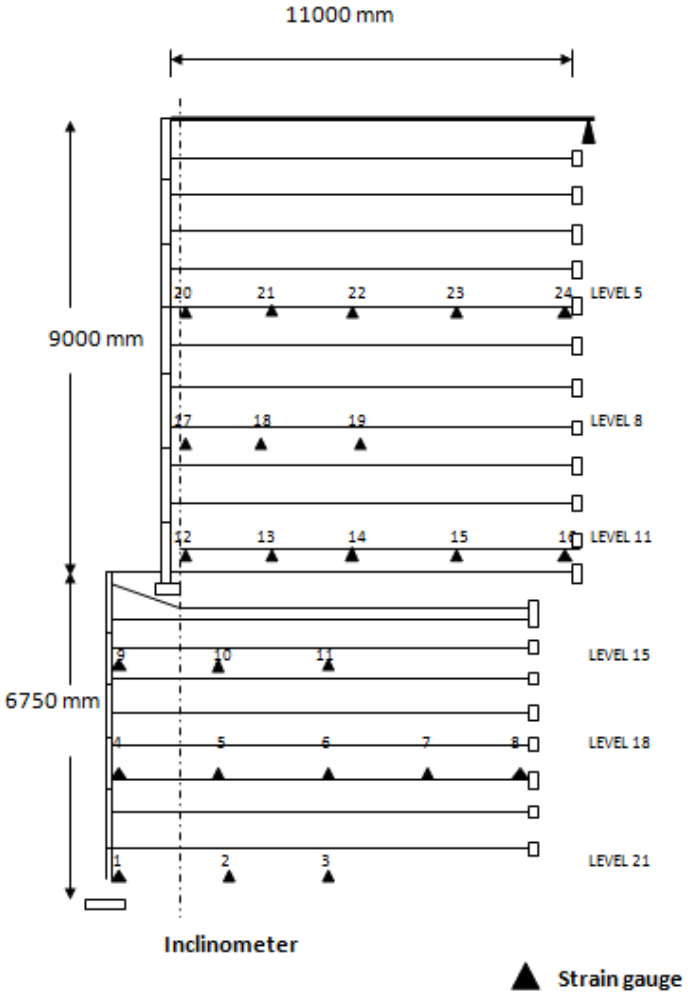

Figure 3. Instrumented section of the multi-anchor wall.

Modeling of reinforcing bars

When assessing the suitability of a particular type of model, it is important to consider the behavior of the reinforcing bars. Reinforcing bars are tensile elements, which are able to carry tensile forces but not compressive forces. Although, the bars exhibit a certain degree of stiffness, they generally behave as flexible elements and hence carry negligible bending stresses. The geotextile element exhibits normal stiffness but not bending stiffness. It can only sustain tensile forces but not compressive forces. Neither does it sustain bending stresses. The tensile force distribution along the reinforcing bar can also be displayed. As such, this element is ideally suited to model the reinforcing bar. The only drawback is that the geotextile is a continuous sheet like structure extends in the out-of-plane direction. In contrast, the reinforcing bars are individual bars. Hence, the forces in the bars are converted into equivalent force per m run in the out-of-plane direction before the geotextile element can be used to model the bar. Despite the drawback, geotextile element is found to be the most suitable model for the reinforcing bar. The effect of compaction on the behavior of retaining wall is significant especially at the upper levels as shown by many researchers (Broms, 1971; Ingold, 1979).

However, the simulation of compaction by the finite element method is not straight forward. Gotteland et al. (1997) attempted to simulate the compaction effect by loading and unloading of a uniform surcharge at the top of wall. This similar approach is used by Kim et al. (2001) and applied to every soil layer. Due to lack of time and the tedium involved in simulating compaction at every incremental lift, the compaction was simulated at the top of the wall. The wall was constructed incrementally. Each lift of panel, backfill and reinforcing bars were installed on top of the earlier lift sequentially. This process was repeated layer by layer until the top of the wall was reached. PLAXIS has the option to simulate stage construction. In this option, the configuration of the geometries was changed by deactivating or reactivating cluster or structural objects. Due to the large height of the wall, there are many lifts in the construction sequence. As a result, it is quite tedious to simulate the actual stage construction sequence. Hence, the wall was simulated monotonically in this study.

VALIDATION OF FINITE ELEMENT MODEL

The validation of finite element model was done by comparing the measured results of the multi-anchor wall with the computed results of the finite element model (Lee, 2004). Field instrumentation was done to measure the behavior of the wall.

Field Instrumentation

Two sections are selected for instrumentation. At one of the sections polystyrene foam is inserted at the back face of the wall panel to allow for lateral deformation to take place. At the other location there is no polystyrene foam insertion, which means that the facing is less flexible in the transverse direction. The instrumented sections are shown in Figure 3. Basically, the instrumentation consists of inclinometer, rod settlement gauge and load measurement along the reinforcing bars at selected levels.

Tensile force distribution

The tensile forces are measured by the strain gauges.

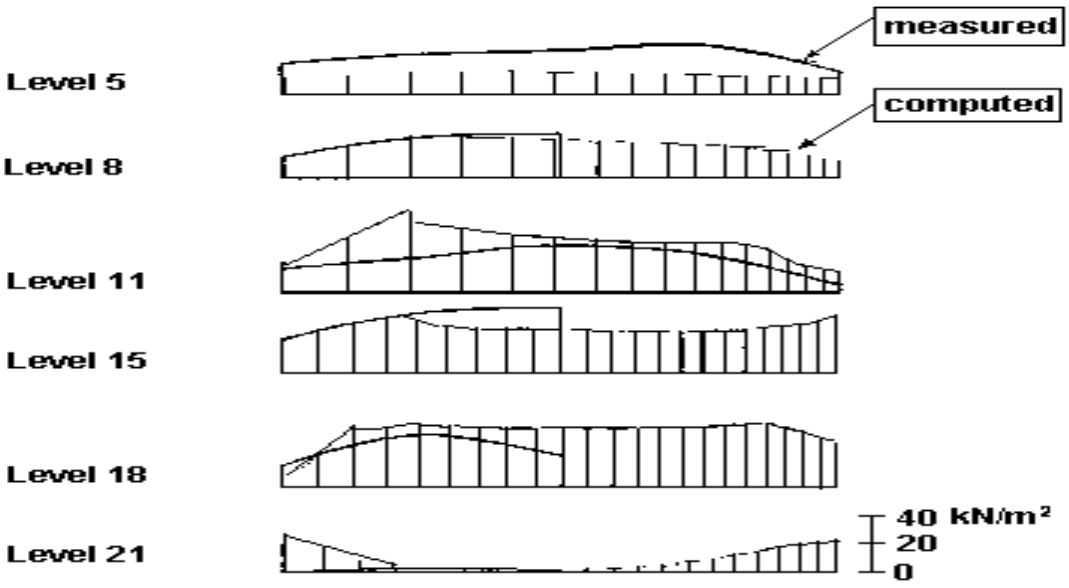

Figure 4. Computed versus measured results along the reinforcing bars.

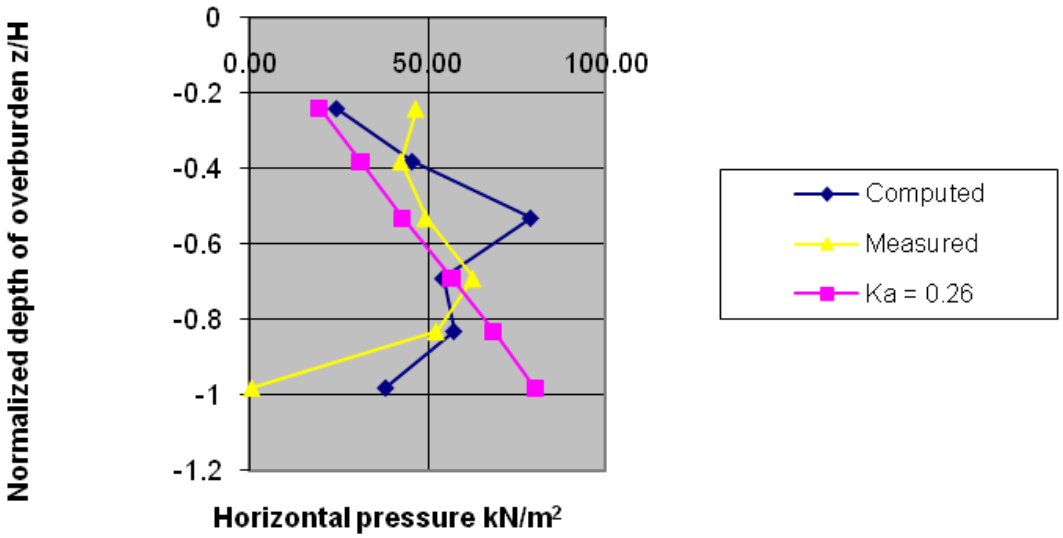

Figure 5. Variation of horizontal pressure with overburden.

The tensile force distribution along the reinforcing bars at each of the instrumented level is shown in Figure 4. For the purpose of comparison, the tensile force distribution is superimposed on the tensile force distribution of the rigid facing. It is seen that the locus of maximum tension is a vertical line offset approximately 0.35H away from the facing. In a tie back system; the tensile force in the reinforcing bar is constant throughout the length of the bar. Hence, the variation of the tensile force along the reinforcing bar confirms that wall is indeed a reinforced soil system rather than a tie back system.

Horizontal pressure distribution

The variation of the horizontal pressure with the normalized depth below the crest of wall is plotted and shown in Figure 5. The Ka line is drawn in the same plot

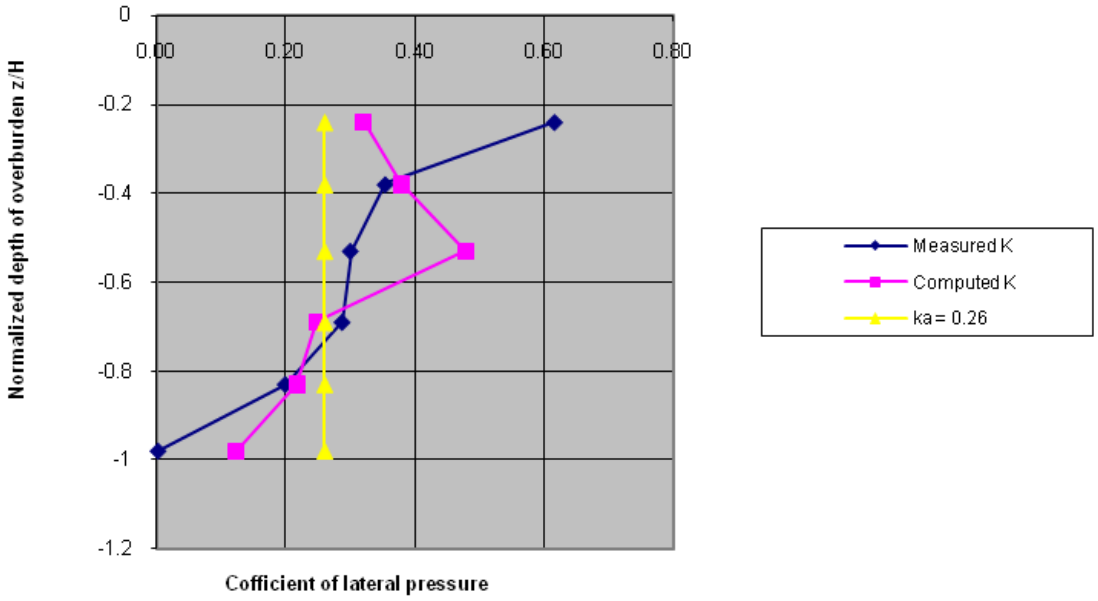

Figure 6. Variation of coefficient of lateral pressure with overburden.

for comparison. Assuming angle of friction of 36°, Ka = 0.26. The explanation for the higher horizontal pressures at shallow depths is that they are induced by the locked in stresses due to compaction. For normalized depth greater than 0.7, the horizontal pressure is below the Ka line. Between the normalize depths 0.4 and 0.7, the horizontal pressures follow closely the Ka line. The approximate parabolic shape of the pressure distribution indicates that perhaps the wall at the toe deforms significantly more thereby resulting in lower horizontal pressure. The variation of coefficient of lateral pressure with depth is plotted as shown in Figure 6. The Ka=0.26 is plotted for comparison. The coefficient of lateral pressure plot tells a similar story as the horizontal pressure plot. For shallow depths that are Dn less than 0.4, the coefficient of lateral pressure far exceeds even the Ka value. Whereas for deeper depth where normalized depth (dn) is greater than 0.8, the K value is far below the Ka value. For dn between 0.4 and 0.8 the K value is pretty well represented by Ka value.

The process of validation involved some trial and error and back analysis. For example, initially the Mohr-Coulomb model was used to model the granular backfill. However, to match the order of magnitude of the lateral deformation of the wall facing, the Young's modulus of the soil had to be reduced to a value that is significantly much smaller than the commonly accepted value for granular soil. In fact, it was subsequently found that the hardening soil model was a better model in simulating the measured results From the above comparison, it is seen that despite some significant discrepancies between the computed and the measured results, the computed results were in general agreement with the measured results. The effects of the compressible layer at the back face of the wall panel were also reasonably well simulated by the finite element modeling. As such, the finite element formulation was suitable to be used for parametric studies to predict the trend and magnitude of the stresses in the reinforcing bars and the deformation characteristics.

INFLUENCE OF LATERAL MOVEMENT AT WALL FACING

The soil at the back face of the wall facing was allowed to move laterally through the introduction of a geoinclusion, which was compressible. In the present parametric study, the compressibility of the geoinclusion as well as its thickness was varied to monitor their effects on the performance of the wall.

Effects of compressibility

The compressibility of the geoinclusion was a function of its E modulus. The E modulus was varied from 300 kN/m^2 to 5000 kN/m^2. The case where there was no geoinclusion was also included for comparison. Where there was no geoinclusion, the maximum tension occurred mostly at the connection. Whereas if the geoinclusion was very compressible that is, where the E

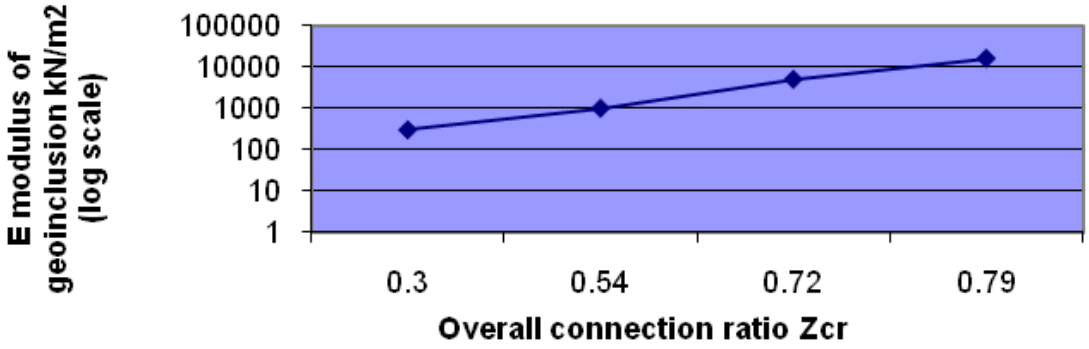

Figure 7. Effect of compressibility on overall connection ratio.

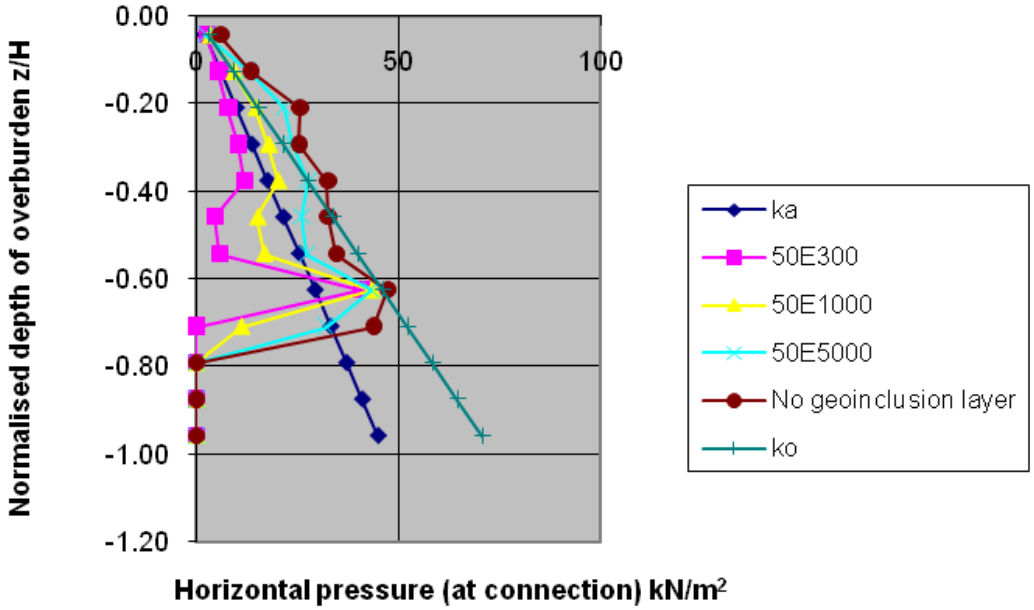

Figure 8. Horizontal pressure at connection versus depth of over burden.

modulus was only 300 kN/m^2, the tension at connection was only a fraction of the maximum. Andrawes and Saad (1994) reported similar behavior for geogrid reinforced walls subjected to controlled lateral deformation. The overall connection ratio Zcr is calculated as follows:

Zcr = Zc/Zt

where, Zcr is the overall connection ratio, Zt, is the summation of maximum tension in all the reinforcing bars. Zc is the summation of tension at all connections at the facing. For the case where the E modulus of the geoinclusion was only 300 kN/m^2, the overall connection ratio was only 0.30. The variation of the E value versus Zcr is shown in Figure 7. The effects of compressibility could further be studied by plotting the horizontal pressures at the connections (that is, at the back face of the facing panel) against the normalized depth of overburden as shown. From Figure 8, it was seen that at E = 300 kN/m^2 for the geoinclusion, the horizontal pressure was significantly below the Ka line. Note that the 50E300 means that thickness of the geoinclusion was 50 mm and the E modulus was 300 kN/m^2. When the E value increased to 1000 kN/m^2, the horizontal pressure line followed more or less the Ka line until when the depth of overburden reached –0.6 H below which the horizontal pressure dropped rapidly to zero. Whereas when there was no geoinclusion, the horizontal pressure line followed more or less the Ko line only until the depth of overburden reached about –0. 7 H below which the

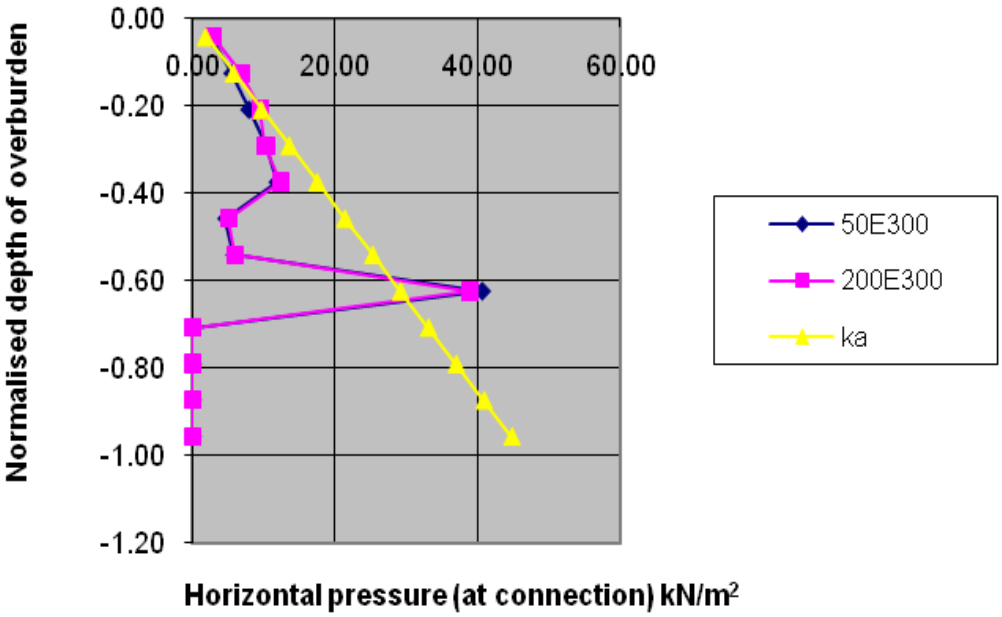

Figure 9. The effect of the thickness of geoinclusion.

horizontal pressure again fall rapidly to zero. It was seen that for all cases, the tension at the connection for the bottom three levels of reinforcing bars was zero. The above observation was more or less concurred by the findings of Andrawes and Saad (1994) based on studies on 2.1 m high geogrid reinforced experimental walls and finite element modeling using CRISP geotechnical finite element program developed by the University of Cambridge (Britto and Gunn, 1990). Andrawes and Saad (1994) find that the use of geoinclusion at the lateral boundary of the wall results in a significant reduction of the horizonal pressures. The horizontal pressure distribution is found to fall well below the K_a line. Where there is no geoinclusion in the lateral boundary, the horizontal pressure distribution is significantly above the K_a line until the overburden reaches –0.7 H below which the horizontal pressure falls below the K_a line.

Effects of thickness of compressible layer

To study the effect of thickness of geoinclusion, the thickness was increased from 50 mm to 200 mm. It was seen from Figure 9 that the horizontal pressure lines for both the cases of 50 mm and 200 mm thick geoinclusion more of less coincide. Hence, it could be concluded that the effect of thickness was insignificant. The maximum horizontal displacements of the wall facing were 87.52 mm and 88.23 mm for 50 mm thick and 200 mm thick geoinclusion, respectively. Hence, from deformation point of view, the thickness of geoinclusion was also not significant. However, Andrawes and Saad (1994) find that the horizontal pressure reduces as the thickness of the geoinclusion increases until the thickness reaches 75 mm beyond which any further increase in thickness would not result in any further reduction in the horizontal pressure. The inability of the PLAXIS to pick up the effects of thickness of the geoinclusion could be due to the relatively small dimension of the thickness compared with the overall height of the wall which is 9 m high. The experimental wall studied by Andrawes and Saad (1994) is only 2.1 m high.

INFLUENCE OF FOUNDATION CONDITION

Effects of compressibility

The effects of compressibility on tension in the reinforcing bars are best seen in the plots shown in Figure 10. In the figure, the horizontal pressure is plotted against the depth of overburden. It was seen that for the least compressible foundation where E=80000 kN/m^2, the maximum horizontal pressure occurred at the normalized depth of overburden of 0.6. As the foundation became more compressible that is, as the E value decreased, maximum horizontal pressure occurred at increasing depth of overburden. When the point of the E value reached 1000 kN/m^2, the point of maximum horizontal pressure occurred at a depth of 0.8. In summary, the effect of increasing compressibility was to lower the point of maximum tension from 0.6 to 0.8 of normalized

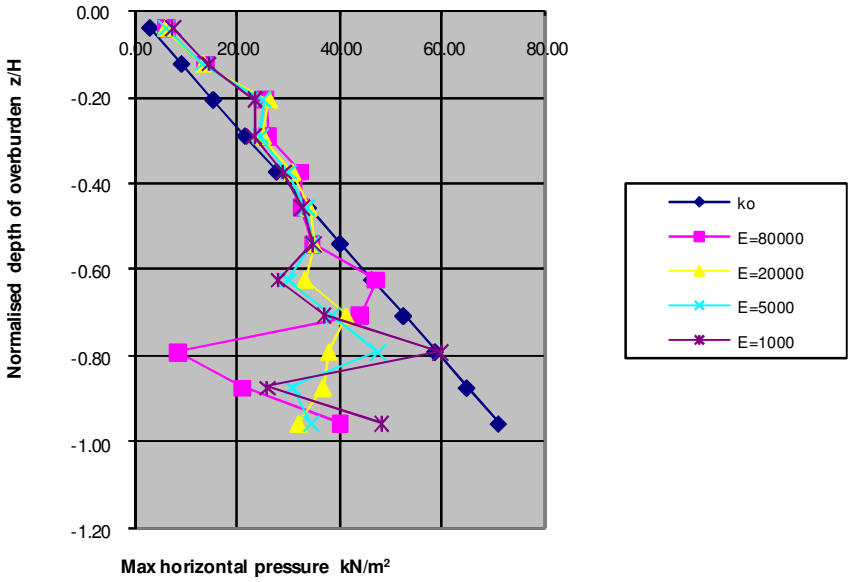

Figure 10. Plot of maximum horizontal pressure versus depth of overburden.

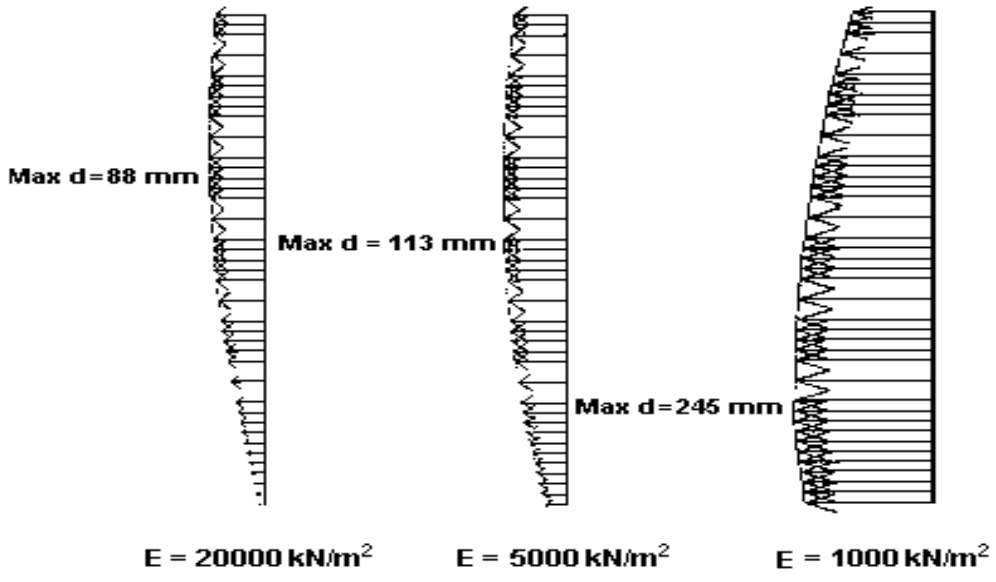

Figure 11. Horizontal displacement of the wall with varying compressibility of the foundation soil.

overburden. Putting it in another way, the yielding of the foundation soil tended to redistribute the stress that resulted in larger tensile forces at the lower levels of the reinforcing bars and smaller tensile forces at around 0.6 overburden level. At upper levels that is, where the overburden was less than 0.5 H, the tensile stresses remained unaffected by the compressibility of the foundation soil. The above behavior is consistent with the general understanding that as the foundation soil becomes more compressible, there is more foundation spreading which would result in greater tension at the lower part of the wall. In Figure 11 the horizontal displacement of the wall facing is shown for various foundation compressibilities. As the foundation became more compressible, the horizontal displacement increased. The point of maximum displacement moved

from the upper part of the wall toward the base of the wall as the foundation became more compressible. Similar trend is reported by Rowe and Ho (1996) whereby forty fold decrease in modulus of foundation soil results in 30% increase in horizontal deformation at the wall face.

CONCLUSION

The above research is carried out to study the influence of boundary conditions on the behavior of Nehemiah wall. The research was done first by formulating a finite element model of the wall. The finite element model was then validated by the measured results of the full scale instrumentation of a 15.75 m high Nehemiah wall. With this validated finite element model, parametric studies were carried out by varying the deformation and loading conditions at three boundaries of a 9 m high Nehemiah wall. These three boundaries were the crest, the facing and the base of the wall. The effects of these boundary conditions on the behavior of the wall were evaluated based on certain stress and deformation criteria. The results and conclusions drawn from these studies are summarized following.

At wall facing

As the geoinclusion becomes more compressible, the overall connection ratio Zcr decreases correspondingly. At E = 300 kN/m^2 for the geoinclusion, the Zcr drops to as low as 0.30. Horizontal pressures at the connection increases with the depth of overburden until a depth of 0.6H is reached. Beyond 0.6H, the horizontal pressure starts to reduce with further depth. In the absence of geoinclusion, the horizontal pressure line follow more or less the Ko line until a depth of 0.6H is reached. Below 0.6H the horizontal pressure starts to drop rapidly. With the insertion of the geoinclusion at the wall facing, the horizontal pressure decreases as the geoinclusion becomes more compressible. The influence of the geoinclusion on the horizontal displacement is relatively small. The influence of the thickness of geoinclusion within the range of 50 to 200 mm is not significant.

At base of wall

The increasing compressibility of the foundation soil induces redistribution of stresses that results in larger tensile forces in the reinforcing bars at lower levels and smaller tensile forces at around 0.6 H depth of overburden. As the foundation becomes more compressible, the horizontal displacement of wall facing increases. The maximum point of horizontal displacement moves from the upper part of the wall facing towards the base as the foundation becomes more compressible.

REFERENCES

Ali FH (1993). Field behaviour of a geogrid-reinforced slope. Geotextiles and Geomembranes, International Geotextiles Society, 12 (1): 53-72.

Ali FH, Adnan A, Chew KC (1992). Use of rice husk ash to enhance lime treatment of Soil. Can. Geotech. J., (29): 843-852.

Ali FH, Osman N (2008). Shear strength of a soil containing vegetation roots. Soils and Foundations. Jap. Geotech. Soc., 48 (4): 587-596.

Anderson WF, Pyrah IC, Ali FH (1987). Rate effects in pressuremeter tests in clays. Geotech. Eng. ASCE, 113:1344 -1358.

Andrawes KZ, Saad MA (1994). Geogrid reinforced soil walls subjected to controlled lateral deformation. 5th International Conference on Geotextile, Geomembranes and Related Products, Singapore.

Britto AM, Gunn MJ (1990). CRISP – users and programmers guide. Cambridge Universty, UK.

Broms BB (1971). Lateral earth pressure due to compaction of cohesionless soils. Proc. 4th Int. Conf. Soil Mech and Fdn. Eng. Budapest., pp.373-384.

Bujang BK Huat, Gue SS, Faisal Hj, Ali (eds) (2008). Tropical residual soils engineering. ISBN 9789058096609.

Gotteland PH, Gourc JP, Villard P (1997). Geosynthetics reinforced structures as bridge abutments: Full scale experimentation and comparison with modelisations. Proc. of the International Symposium on Mechanically Stabilized Backfill. Denver, USA, pp. 25-34.

Ingold TS (1979). The effects of compaction on retaining walls. Geotechnique, 29: 265-283.

Jones CJFP, Pugh RC (2001). A full-scale field trial of electrokinetically enhanced cohesive reinforced soil using electrically conductive geosynthetics. Proc. Inter. Symp.on Earth Reinforcement. Japan: pp. 219-224.

Kim YY, Han KJ, Kim KM (2001). A field instrumentation and FEM analysis for an isolated-reinforced earth wall. Proc. of the Inter. Symp. on Earth Reinforcement, Japan: pp.381-386.

Lee CH (2004). Influence of boundary conditions on the behaviour of a reinforced soil wall. Ph.D Thesis, University of Malaya (unpublished).

Normaniza O, Faisal HA, Barakbah SS (2008). Engineering properties of *Luciana leucocephala* for prevention of slope failure. Ecol. Eng., 32: 215-221.

Rowe RK, Ho SKP (1996). Some insights into reinforced wall behavior based on finite element analysis. Proc. of the Int. Symp. on Earth Reinforcement. Japan, pp. 485-490.